HEFAT2014
10th International Conference on Heat Transfer, Fluid Mechanics and Thermodynamics
14 – 16 July 2014
Orlando, Florida

COMBINED PLIF-IR THERMAL MEASUREMENTS OF WAVY FILM FLOWS UNDERGOING FORCED HARMONIC EXCITATION

Mathie, R. Charogiannis, A. and Markides C.N.*
*Author for correspondence
Department of Chemical Engineering,
Imperial College London,
United Kingdom,
E-mail: c.markides@imperial.ac.uk

ABSTRACT

A combined PLIF/IR thermography technique was developed and employed towards the measurement of unsteady and conjugate heat transfer in thin, gravity-driven falling liquid film flows (with and without flow pulsation) over an inclined heated metal foil. Simultaneous, local film thickness, film and substrate temperature, heat flux exchanged with a heated foil and heat transfer coefficient results are reported for a range of electrically applied heat input values, flow Reynolds (*Re*) numbers and flow pulsation frequencies. Moreover, interfacial wave velocities were calculated from cross-correlations across successive thickness profiles. Results concerning the instantaneous and local heat transfer coefficient variation and how this is correlated with the instantaneous and local film thickness variation (waves) suggest that the heat transfer coefficient experiences an enhancement in thinner films. The particular observation is most probably attributed to a number of unsteady flow phenomena within the wavy fluid films that are not captured by the steady analysis. At low flow *Re* number values the mean Nusselt (*Nu*) was around 2.5, in agreement with laminar flow theory, while at higher *Re* values, higher *Nu* were observed. Finally, lower wave amplitude intensities were associated with higher heat transfer coefficient fluctuation intensities.

INTRODUCTION

The present paper describes a series of experiments dedicated to the study of unsteady and conjugate heat transfer in heated, gravity-driven falling films [1, 2]. In particular, spatiotemporally resolved heat transfer measurements were carried out by employment of a combination of non-intrusive optical diagnostics in interfacial film flows of water-ethanol mixtures falling down a heated metal foil. Planar laser Induced Fluorescence (PLIF) was utilized alongside Infra-Red (IR) thermography in order to simultaneously recover film thickness, interfacial velocity, film free-surface and substrate temperature data, and obtain local and instantaneous and local heat flux and heat transfer coefficient (HTC) information.

NOMENCLATURE

α	[μm]	Foil thickness
α_n^*	[-]	Normalized foil thickness
c	[J K^{-1}]	Heat capacity
d	[mm]	Film thickness
D	[mm]	Film depth
h	[W $m^{-2}K^{-1}$]	Heat transfer coefficient
k	[W $m^{-1}K^{-1}$]	Thermal conductivity
Nu	[-]	Nusselt number
Pr	[-]	Prandtl number
$\dot{q}$	[W cm^{-2}]	Heat flux
Re	[-]	Reynolds number
t	[s]	time
T	[K]	Foil temperature
v	[m^2 s^{-1}]	Kinematic viscosity
x	[mm]	Stream-wise direction of the flow
z	[mm]	Distance along the span-wise direction of the flow
Special characters		
a	[m^2 s^{-1}]	Thermal diffusivity
Γ	[m^2 s^{-1}]	Flow rate per unit width
δ	[μm]	Thermal diffusion length in the solid
ΔT	[T]	Temperature difference
ε	[-]	Foil emissivity
ε_s	[W $s^{-1}K^{-1}m^{-2}$]	Foil effusivity
σ_h	[W $m^{-2}K^{-1}$]	Standard deviation of the HTC fluctuation
ρ	[m]	Density
ω	[s^{-1}]	Harmonic of the temperature fluctuations
Subscripts		
app		Apparent: In reference to the foil temperature
bg		Background: In reference to the foil temperature
f		Fluid
IR		Infra-Red
n		n^{th} harmonic of the temperature fluctuations
s		Solid
u		Underside: In reference to the foil temperature
w		Wall

Gravity-driven heated falling films, which stand for the focal point of the current investigation, are employed in a wide range of industrial processes such as wetted-wall absorbers, condensers, evaporators and reactors, owing to their high surface-to-volume ratios and associated heat and mass transfer capabilities even at modest flow rates. Extended theoretical and experimental investigations suggest that the rates of heat and mass transfer are strongly linked to the spatiotemporal variation of the hydrodynamic characteristics of these films, and in particular, the waviness of the gas-liquid interface [3-5].

In order to reveal the underlying unsteady flow phenomena, optical diagnostics have been extensively employed in the study of such flows, as they allow for non-invasive, real-time imaging of flow features such as the film thickness and interfacial velocity [6, 7]. Despite their inherent capabilities, the application of optical techniques in heated film flows is particularly challenging; as the liquid is in physical and thermal contact with a hot solid substrate which is typically metallic and opaque, illumination of the liquid domain from the solid side is often unfeasible, with the liquid free surface providing the only optical access. In that case, refraction by the wavy interface results to strong beam steering that can seldom be accounted for.

Beyond quantifying local film thickness fluctuations, the study of diabatic (heated/cooled) film flows entails liquid temperature measurements, commonly obtained by fluorescence imaging techniques employing temperature-sensitive markers. Such measurements are also subjected to the aforementioned challenges, and any available studies are consequently limited to single point measurements. Amongst others, the exemplary efforts by a group in Aachen [8, 9] to conduct simultaneous film thickness and temperature measurements by employment of diacetyl fluorescence and phosphorescence imaging need essentially be noted. In more detail, time-varying local HTCs were reported relative to the measurement position (+ 80% ahead and - 40% below the wave crest), suggesting a strong correlation between the film thickness and heat transfer. Unfortunately, the particular experimental effort was restricted to a narrow flow parameter range (single Reynolds number of 126), while the wave regime was not identified. Moreover, the results were recovered on the assumption that the velocity within the film is well-described by the theoretical Nusselt profile [10]. Deviations from this ideal profile on account of two and three-dimensional unsteadiness have, however, been confirmed [11].

Part of our growing insight into the complex unsteady phenomena associated with thin film flows can be attributed to the extensive body of experimental research carried out by the Russian Academy of Sciences [12-15] and a group at Darmstadt [16]. This work, however, is mostly dedicated to either reporting time-averaged HTCs, or the characterization of hydrodynamic flow regimes in the case of the former. It should essentially be noted that amongst the extensive bulk of relevant publications, the hereby sighted experimental work is the one specifically associated with the application of optical techniques and IR thermography. The latter has been extensively employed in free-surface temperature measurements, a prerequisite of which is the high absorptivity of the imaged liquid. In order to allow for surface temperature measurements devoid of contributions from the liquid bulk, the absorption coefficient over the sampled spectral region must be high enough so that only the radiation from a thin (few micrometres) layer is collected by the detector (IR camera) [17]. Amongst others, the use of IR thermography in water film provides an exemplary illustration of the utility of the particular method in relevant experimental studies [18, 19].

EXPERIMENTAL METHODS

The experimental methods developed and employed in the present campaign are described in greater detail in references [1, 20], along with the calibration and methodology verification procedures. For this reason, only a short summary will hereby be provided, with the main body of the paper focusing on the obtained qualitative and quantitative results.

The objective of the undertaken experimental effort is to measure the instantaneous temperature and heat flux of aqueous (water-ethanol) solutions forming thin films as they flow down a flat, inclined heated titanium foil (thickness a = 50 μm). The foil was heated by applying a current from a DC power supply with a maximum heat flux capability of 4.2 W cm^{-2} over the 1,200 cm^2 foil area. The liquid flow was uniformly distributed over the heated foil by means of a 0.3m wide knife-edge positioned at the exit of the flow distribution box. The film flow was comprised of two components, a steady and an unsteady, the latter corresponding to a prescribed proportion of the former which was by-passed and pulsated. The pulsating component of the flow was modulated by a rotating throttle valve in order to selectively excite coherent large-scale waves.

Once a flow condition was established, a PLIF technique based on the temperature-dependent Rhodamine B (Rh-B) fluorescence was used to identify the film free surface location and measure the film free surface temperature. A simplified schematic representation of the optical setup is provided in Figure 1.

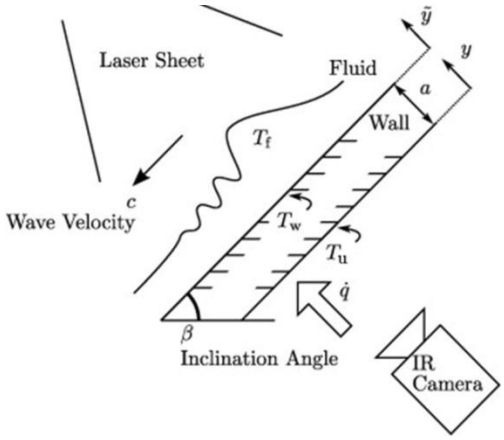

Figure 1: Schematic representation of the heated film flow experiment. PLIF measurements were carried out both along as well as across the flow direction. Reproduced from ref. [1].

The dye-doped aqueous flow was excited by a 100 μm thick planar laser sheet, generated by dedicated light sheet optics and originating from a dual-cavity, frequency-doubled (532 nm) Litron Nd:YAG laser, operated at 100 Hz. The red-shifted Rh-B fluorescence emission was captured by a pair of synchronised 1,280 × 1,024 pixel LaVision CMOS cameras equipped with optical long-pass dichroic/interference filters (540 nm cut-off wavelength). A two-camera setup was adopted in order to expand the field of view and increase the effective spatial resolution of the imaging system. The spatial resolution of the LIF setup was 28.7 μm/pixel. LIF measurements were performed along both the stream and span-wise directions of the flow, while a pinhole model calibrated using an image calibration graticule, was employed in correcting the raw images for perspective distortion relative to the excitation plane. A number of methods were devised for systematically detecting the film free surface location, with a gradient method adopted for producing the smoothest results. The LIF intensity dependency on temperature was calibrated during independent runs using thermocouples, with the resulting root-mean-square (RMS) error between the thermocouple and PLIF measurements being 0.5 K. A typical film PLIF image is shown below (Figure 2). In this case, the x-axis corresponds to the stream-wise flow direction whereas the y-axis cuts across to the liquid film depth. Owing to the combined effects of the gas-liquid interface waviness and the change in the refractive index, PLIF image are strongly distorted; squeezed (in the y-direction) while the solid-liquid interface follows the gas-liquid interface waviness. Therefore, the real location of the solid-liquid interface was identified prior to introducing a liquid flow, using a calibration graticule and the pinhole camera projection model available by the LaVision software package (Davis).

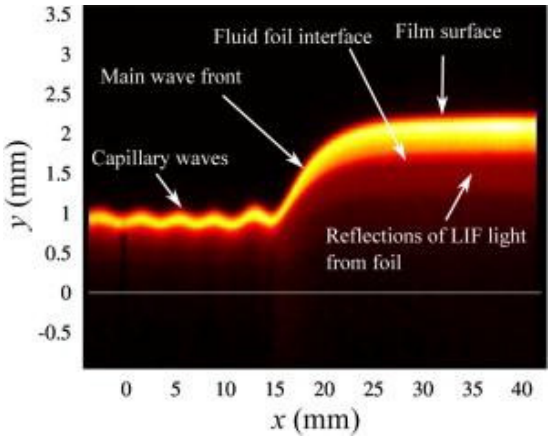

Figure 2 PLIF image of the wavy interface corrected for perspective distortion relative to the excitation plane, reproduced from ref. [1].

Simultaneous to the collection of PLIF images, temperature measurements were made on the underside of the foil using an IR camera, as well as the fluid inlet (distribution box) using thermocouples. Two IR cameras were employed in the present work depending on availability; a long-wave (LWIR) FLIR SC3000, and a mid-wave (MWIR) Cedip Titanium. An IR camera measures the incident radiation flux, which is partly comprised of the radiation emitted by the foil itself, and partly by background radiation reflected off the foil surface. Contributions of the latter were minimized by obscuring the area that would have been in the line-of-sight of the camera as a result of specular reflections, using thick black card paper with near-unity emissivity. The resulting signal, now comprised of the foil and background radiation associated with the black card paper screen, was converted to an apparent foil temperature T_{app} using Equation (1).

$$T_{app}^{\ 4} = \varepsilon T_u^{\ 4} - (1-\varepsilon) T_{bg}^{\ 4} \quad (1)$$

Thermocouple measurements and thermal targets of known emissivity allowed for the true foil temperature T_u to be determined, by correcting for the foil emissivity ε and background signal contributions T_{bg}.

Similar to PLIF, raw IR camera images were also corrected for perspective distortion. An affine matrix transformation method was devised for this purpose, as well as for spatially aligning the PLIF and IR imaging region. The alignment mismatch is estimated to be less than 2 mm. A typical example of a corrected IR image of the foil underside is provided in Figure 3.

Figure 3: Instantaneous temperature distribution of the foil underside illustrative of the flow thermal traces as obtained by the FLIR SC3000 camera at conditions of Re = 360, heat flux of 2.1 Wcm^{-2} and pulsation frequency of 1.76 Hz. The vertical axis corresponds to the stream-wise direction while the horizontal to the span-wise direction. From dark to bright, the colour scale represents cool to hotter regions.

The final step in the IR image processing routine is to recover the temperature and heat flux on the wetted side of the foil using images corrected for background radiation, foil emissivity and perspective distortion, from the back side of the foil. In order to fulfil this purpose, the foil thickness was selected to be over an order of magnitude lower than any thermal feature observed by the IR camera, with the resulting heat transfer assumed to be dominated by 1-D conduction through the foil thickness. A 1-D thermal conduction model with constant heat generation (through resistive heating) was developed and used to describe the thermal response of the foil to temperature fluctuations on solid-liquid interface, with an adiabatic boundary condition imposed on the foil underside. The corresponding thermal response relating the liquid-solid

interface temperature $T_{w,n}$ to the measured temperature fluctuations on the underside of the foil $T_{u,n}$ of a given frequency is provided by:

$$T_{w,n} = T_{u,n} \cosh\left\{(1+i)\alpha_n^*\right\} \quad (2)$$

The heat flux response $\dot{q}_{w,n}$ is provided by:

$$\dot{q}_{w,n} = \left[(1+i)\varepsilon_s(\omega n/2)^{1/2}\right]T_{u,n} \sinh\left\{(1+i)\alpha_n^*\right\} \quad (3)$$

Here, $\alpha_n^*=\alpha/\delta_{s,n}$ stands the foil thickness α normalized to a thermal diffusion length in the solid $\delta_{s,n}=(2\alpha_s/\omega_n)$, associated with the n^{th} harmonic of the fluctuations, α_s stands for the thermal diffusivity of the solid, $\varepsilon_s=(k_s\rho_s c_s)^{1/2}$ for the thermal effusivity of the solid, and k_s, ρ_s and c_s for the thermal conductivity, density and heat capacity.

Two important experimental parameters relevant to this study are the Re and Nu numbers. The former, defined as the ratio of inertial to viscous forces, is calculated based on the average flow velocity in the distribution box U_{box}, the depth of the channel formed by the distribution box knife edge and foil D, and the fluid kinematic viscosity ν_f. The product $D\cdot U_{box}$ is equal to the flow rate per unit width of the channel Γ.

$$\mathrm{Re} = \frac{DU_{box}}{\nu_f} = \frac{\Gamma}{\nu_f} \quad (4)$$

The Nusselt number, which provides the ratio of convective to conductive heat transfer, is defined in terms of the heat transfer coefficient h, the film thickness d and fluid conductivity k_f.

$$\mathrm{Nu} = \frac{hd}{k_f} \quad (5)$$

RESULTS AND DISCUSSION

Free-surface thermal features of films without pulsation

Selected instantaneous results pertinent to the formation and interaction of rivulet structures on the heated falling film free-surface are displayed in Figures 4 and 5. Figure 4 reveals regularly spaced, finger-like structures forming in close vicinity to the flow inlet, and developing along the direction of the flow (x-direction, positive from top to bottom), while quantitative film height and film free surface temperature data (recovered by both IR thermography and PLIF imaging) corresponding to the 50 mm slice indicated in Figure 4, are presented in Figure 5. The following remarks are made: The agreement between the two optical techniques regarding the surface temperature measurement is rendered satisfactory, with the main thermal features identified and adequately resolved by both. The film is thicker where the surface temperature is lower and vice versa, with the two troughs in the film thickness measurement corresponding to the two larger peaks in the surface temperature measurement. Note that no film thickness trough corresponding to the shorter peak, the latter captured by both imaging techniques, is identified, an observation (i.e. clearly discernible thermal features observed over flat film regions) encountered consistently in these experiments.

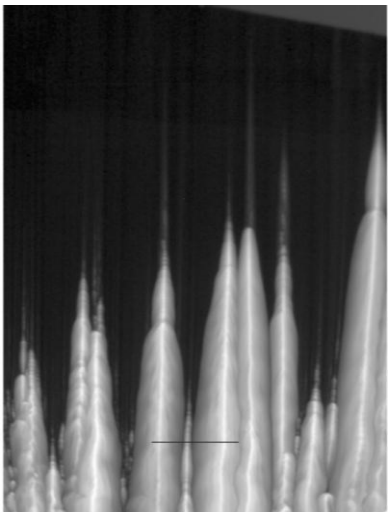

Figure 4: IR image of the liquid film free-surface at Re = 179, heat flux of 3.5 W cm^{-2}, and no flow pulsation. The vertical axis corresponds to the stream-wise direction while the horizontal to the span-wise direction. From dark to bright, the colour scale represents cooler to hotter regions. The 50 mm long black line near the bottom of the image indicates the PLIF measurement location (x = 285 mm downstream of the flow inlet) corresponding to Figure 5.

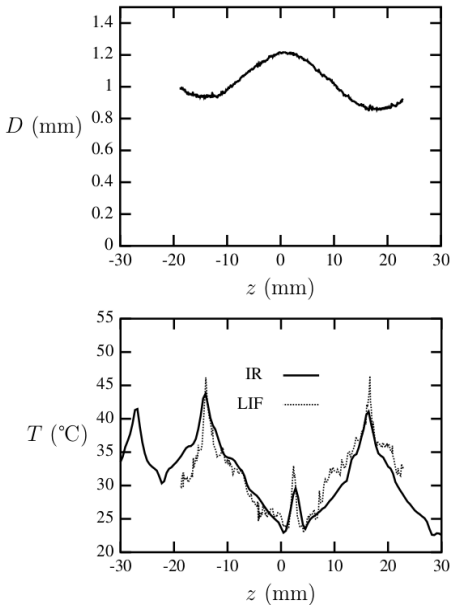

Figure 5: Film thickness (top) and free-surface temperature (bottom) obtained by PLIF and IR imaging at Re = 179 and an imposed heat flux of 3.5 W cm^{-2}. The obtained profiles correspond to a horizontal slice along the film width at x = 285 mm downstream of flow inlet. The z-axis indicates the span-wise direction of the flow.

The advent of flat, "hot" rivulet structures, such as the one discussed above, is believed to manifest itself in the

development of Marangoni flows at the film surface, driven by temperature-induced surface tension gradients. In more detail, the local temperature rise is believed to trigger instabilities at the film thickness, and the ensuing (Marangoni-driven) mass transfer, characterized by accumulation of fluid in the cooler regions, and thinning at the hotter ones. In that way, the rivulets whose origin can be found further upstream (larger structures of Figure 4) might have evolved in this manner.

The spatial evolution of the aforementioned thermal features is examined in Figure 6, where temperature profiles obtained by the IR camera are displayed for different axial locations along the flow. The observed temperature gradients across the film free surface (z-axis) increase with increasing distance from the flow inlet (x-direction), reaching a maximum at the bottom-most measurement location (x = 285 mm).

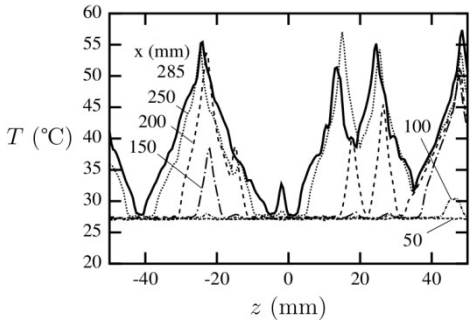

Figure 6: Instantaneous temperature profiles across the liquid film surface, extracted from a single IR image at different stream-wise locations from the knife-edge. The flow and heating conditions are: Re = 179 and 3.5 W cm^{-2} respectively.

Having provided an account of the spatial evolution of the observed finger-like thermal features developing over the film free surface, their temporal variation is examined in Figure 7. In particular, an oscillatory behaviour with respect to the stream-wise flow direction was identified, potentially contributing to the heat transfer enhancement mechanism through boosted mixing. In more detail, the high surface temperature fluid region appears to move up and down along the flow direction with an approximate period of 1 s, with the originally thin rivulet growing wider and moving upstream (0.0 – 0.5 s), reaching a maximum extent at around 0.5 s, and finally being washed back down with its edge becoming blunter until the cycle repeats.

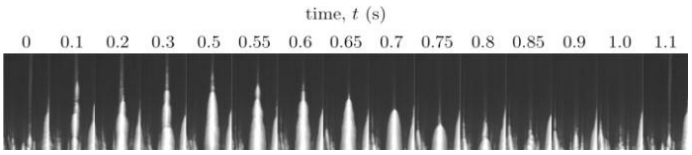

Figure 7: Oscillatory rivulet motion along the stream-wise direction of the flow , imaged over 1.1 s at Re = 251, electrically imposed heating of 2.4 W cm^{-2} flux, and no flow pulsation.

Greater insight into the effects of fluid flow rate and applied heat flux on the film thermal features developing over both the free-surface and solid-liquid interface, the latter as a result of conjugation, is provided by inspection of the ensuing temperature distributions (Figure 8). Here, the flow Re varies between 107 and 251, while the heat flux is adjusted in the 0.1 – 3.47 W cm^{-1} range. The straight, streak-like peaks in the fluid temperature once again appear as a regular equispaced pattern along the flow direction, as do their corresponding footprints in the foil underside. It should finally be noted that the presented distributions of the foil underside and liquid film free-temperature were not collected simultaneously; instead, the IR camera was relocated on top of the setup once the desired range of experimental conditions was investigated, and the same conditions were reproduced.

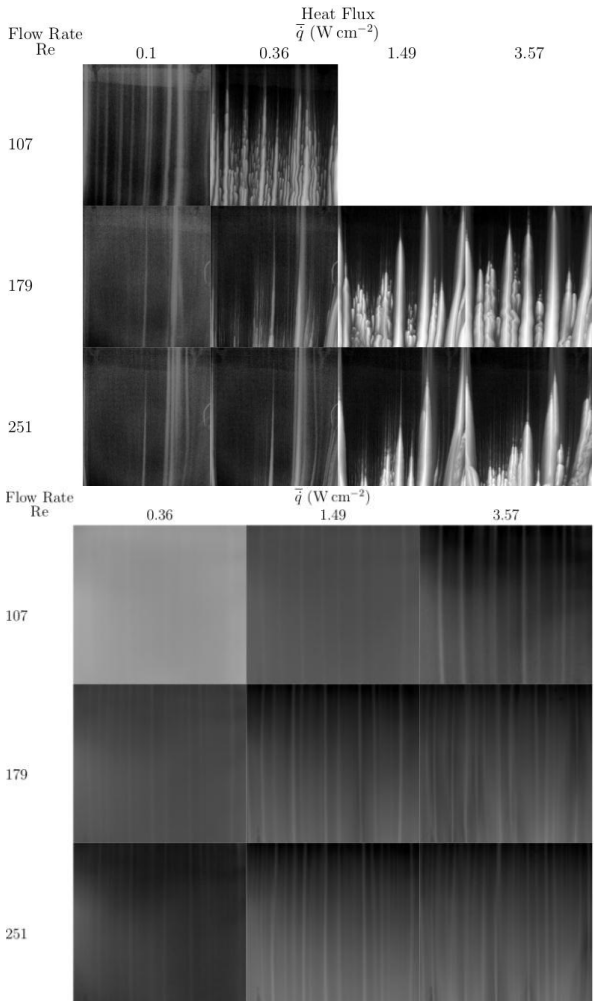

Figure 8: Temperature distribution of the liquid film free-surface (top) and foil underside (bottom) at different flow Re values (107, 179 and 251) and heat fluxes (0.1, 0.36, 1.49, 3.57 W cm^{-2}), as measured with the IR camera. The inclination angle was set to 40° and the liquid was comprised of 20% ethanol/water b.v.

Increasing either the flow rate or heat flux boosts the spatial frequency (in the span-wise direction) and amplitude of these features in both measurement domains. From intermediate Re numbers, the aforementioned oscillatory behaviour of these

streaks also becomes evident. For the same applied heat flux, the streak pattern moves downstream with increasing Re, while for the same Re, increasing the heat flux triggers the opposite trend. It should finally be noted that the frames at low Re and high heat fluxes at the topmost part of Figure 8 are missing as the corresponding flow conditions could not met without risking irreversible damage to the foil due to dewetting.

Free-surface thermal features of pulsed films

Flow pulsation was instigated over a range of experimental conditions in order to generate hydrodynamic waves and thus, allow for more controllable and coherent amplitude and frequency fluctuations in the HTC (Figure 9).

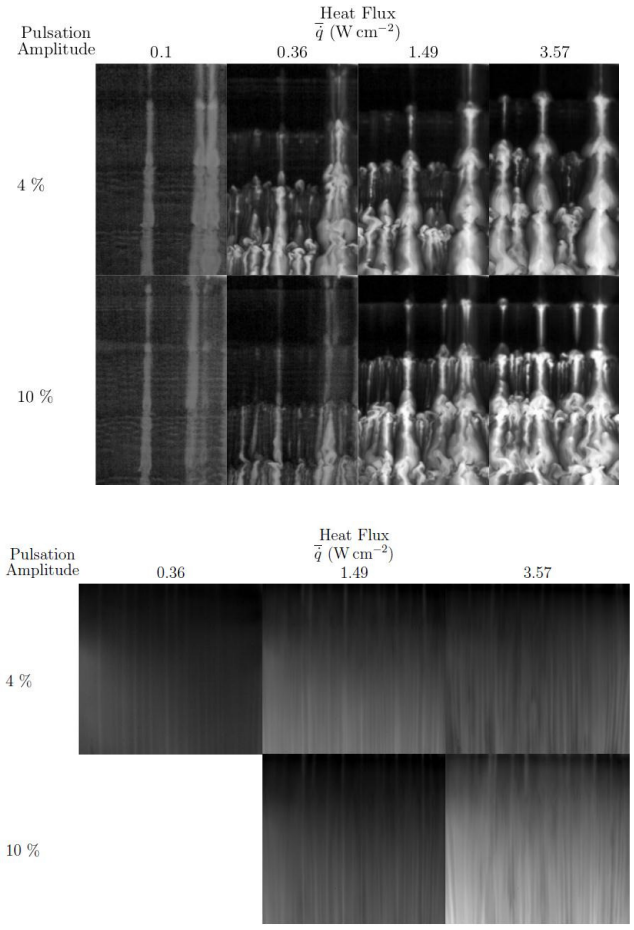

Figure 9: Temperature distribution of the liquid film free-surface (top) and foil underside (bottom) at Re = 179, and the same range of imposed heat fluxes (0.1, 0.36, 1.49, 3.57 W cm^{-2}), foil inclination angle (40°) and fluid composition (20% ethanol/water b.v) as in Figure 8. The pulsation frequency was set to 1.8 Hz, while two different pulsation amplitudes (4% and 10% of the mean flow) were examined.

Temperature distributions for the flow free surface and foil underside are hereby presented for two pulsation amplitudes (4% and 10% of the mean flow rate), a pulsation frequency of 1.8 Hz and a Re number of 179. The fluid composition (20% b.v. ethanol in water), inclination angle (40°), and range of electrically applied heat fluxes were also carried over from the unpulsed study. Looking at both the free-surface and foil underside temperature distributions, it is apparent that the presence of hydrodynamic waves enhances mixing between hot regions and the adjacent colder fluid. Whereas at lower heat fluxes and pulsation amplitudes the spatial regularity of the rivulets structures (compared to the unpulsed case) is reproduced, at higher pulsation frequencies and heat fluxes the rivulet morphology is substantially more random in character.

Film thickness/heat transfer coupling

The temporal evolution of the film depth D (far left) and film free surface temperature T_{LIF} measured by the PLIF technique (second from left), foil temperature T_{IR} measured by the IR camera at the same location (second from right), and foil temperature at 285 mm downstream of the flow inlet (far right), is presented in Figure 10 over a 1.8 s time interval. In these experiments, the PLIF cameras were positioned at 185 mm downstream of the flow inlet in order to image a region along the film span, the imposed heat flux was set to 3.58 W cm^{-2}, the flow Re to 179, and the foil inclination angle to 40°. As was reported earlier (Figure 5), film troughs are observed in regions of high film free-surface temperature. Here, one can associate this local thinning, resolved in space and time, with the brighter (higher temperature) regions in the foil underside image. Moreover, the film depth map shows a trough developing between t = 0.1 s and 0.6 s, and reappearing at around t = 1.3 s. This oscillatory behaviour is believed to correspond to the one noted earlier (Figure 7). While the trough oscillates up and down along the stream-wise direction of the flow, faint "bow-like" features appear ahead of and along its periphery. The same features are also apparent as the flow Re is increased to 251 (Figure 11).

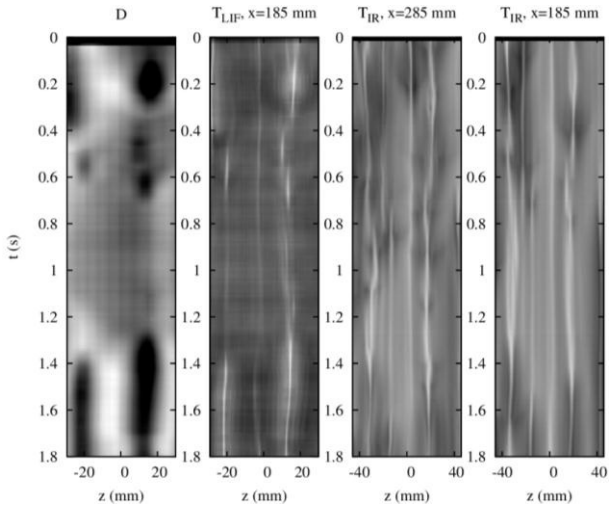

Figure 10: Comparison between the PLIF film depth D and surface temperature T_{LIF} measurements, and IR temperature measurements on the foil underside T_{IR}, at Re = 179, imposed heat flux of 3.58 W cm^{-2}, and no flow pulsation. Results are shown at distances x = 185 mm and 285 mm (for T_{IR} only) downstream of the flow inlet.

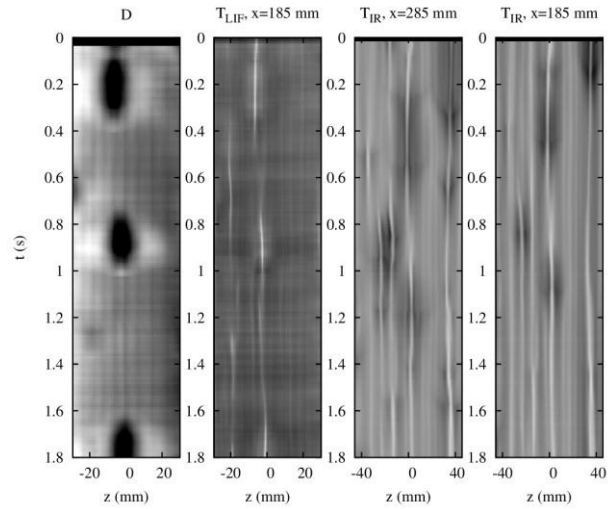

Figure 11: Comparison between the PLIF film depth D and surface temperature T_{LIF} measurements, and IR temperature measurements on the foil underside T_{IR}, at Re = 251. All other experimental conditions correspond to those of Figure 10.

In Figure 12, the time evolution of the instantaneous heat flux, HTC and Nu number are displayed over the same time interval and same spatial location as in Figure 10.

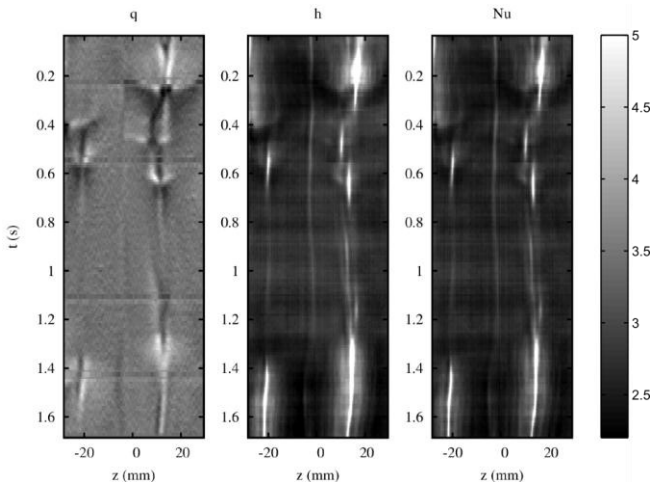

Figure 12: Instantaneous local heat flux q, heat transfer coefficient h, and Nusselt number Nu corresponding to the film thickness and interfacial temperature measurements presented in Figure 10 (Re = 179, heat flux of 3.58 W cm^{-2}, no flow forcing). The heat flux variation was approximately 4%, the HTC varied in the range 1,000 – 3,000 W m^{-2} K^{-1} range, and the average Nusselt number was Nu ~ 2.8.

As expected, the Nu number and HTC are highest where the film is thinnest, while the aforementioned "bow-like" features are once again evident.

Coupling between the film thickness and HTC was also observed when performing quantitative instantaneous measurements along the flow direction. In Figure 13 (top), for example, spatial snapshots of the film thickness of an advancing wave preceded by smaller capillary waves is plotted at five consecutive instances. Along with the film thickness d, measurements of the temperature difference across the film thickness ΔT_f , and heat transfer coefficient h, as determined over the 40mm imaged domain are also presented. Similar to the previously described experiments, the instantaneous local ΔT_f and HTC are augmented in the thinner film regions, while small amplitude fluctuations are captured even in the capillary wave region. Looking at the lower part of the figure where time traces of the local film thickness d, heat transfer coefficient h, fluid and wall temperature T_f and T_w, and heat flux $|\dot{q}_w|$ are presented over a 1 s time interval, the periodic variation of all experimentally determined quantities can be observed.

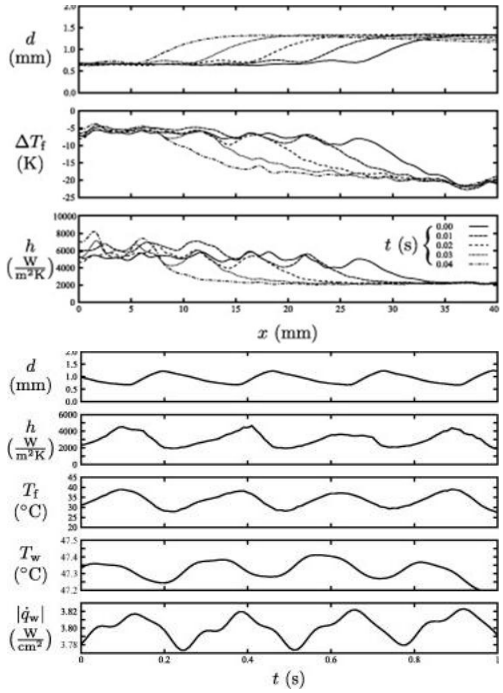

Figure 13: (Top) Spatial snapshots of the film thickness d, temperature difference across the film thickness ΔT_f, and heat transfer coefficient h, of an advancing wave taken from reference [1]. (Bottom) time traces of the instantaneous film thickness d, heat transfer coefficient h, fluid and wall temperature T_f and T_w, and heat flux $|\dot{q}_w|$ data over a 1 s sampling period at Re = 300.

Aggregate heat transfer characteristics

Joint probability density functions (PDFs) of the instantaneous local HTC and Nusselt number Nu against film thickness for 12 runs conducted under the same flow conditions (Re = 300) and varying heat input levels (200 – 5000 W) are presented in Figure 14. Along with the experimental data, the steady flow Nusselt relationship is also included in the plot. Despite following similar trends, the experimental data display significantly higher HTC values (by up to a factor of 2) compared to the steady predictions, most probably due to a number of unsteady flow processes not captured by the steady analysis.

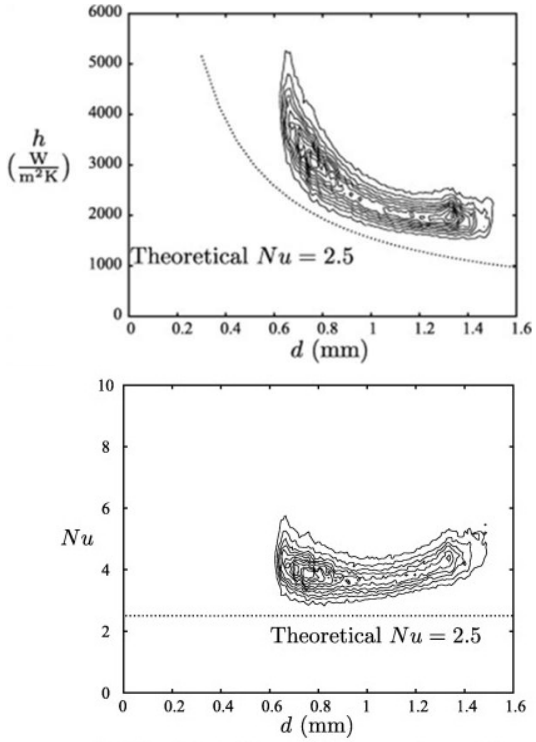

Figure 14: Joint PDFs of the instantaneous local HTC and Nusselt number Nu plotted against film thickness for data acquired over 12 runs, and carried out under the same flow conditions (Re = 300) but with heat input levels varying between 200 W and 5 kW (figure reproduced from ref. [1]).

Further insight into the effects of unsteadiness on the HTC can be obtained by examining PDFs generated from data corresponding to different flow conditions (Re numbers):

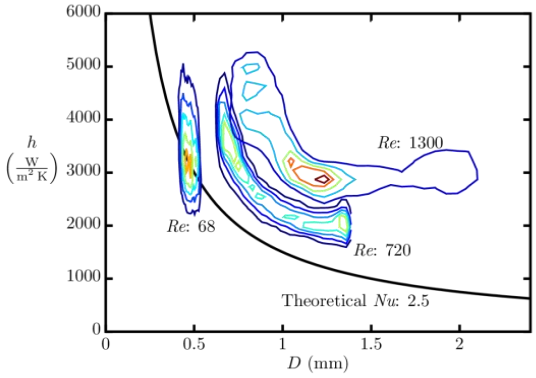

Figure 15: PDFs of the HTC plotted against film thickness for data acquired under three different flow conditions: Re = 68, Re = 720 and Re = 1300.

In the case of the lower Re number study (Re = 68), the majority of the experimental data follow the theoretical Nusselt description. As the Re number increases to 720, the trend observed earlier in Figure 14 is reproduced, with the experimentally determined HTC values being globally higher that predicted ones. Moreover, the HTC dependence on the film thickness becomes weaker than anticipated by the analytical Nusselt solution at higher film thicknesses. Further increasing the Re number to 1300 boosts the observed HTC values even more, and accentuates the previously noted observation, with the HTC appearing almost decoupled from the film thickness.

The formerly noted deviations from the Nusselt theory prediction are re-examined in Figure 16, where the mean flow Nu number is plotted against the mean flow Re number over a range of pulsation amplitudes and frequencies. Along with the experimentally determined data points, a correlation produced by Wilke [21], linking the heat transfer coefficient, Prandtl number Pr and Re number in heated falling films is also presented. Close inspection of Figure 16 reveals that whereas the lower Re number data points (below around 200) fit closely the value predicted by the Nusselt theory (Nu = 2.5), intermediate and high Re number flows display significantly higher Nu numbers, matching Wilke's correlation closely when the latter is expressed in terms of the mean flow Nu number. A possible explanation for this substantial heat transfer enhancement, as observed in both experimental investigations [22] and also verified by modelling efforts [23], is stronger mixing and enhanced convective effects in the main wave regions, associated with emergence of recirculation zones.

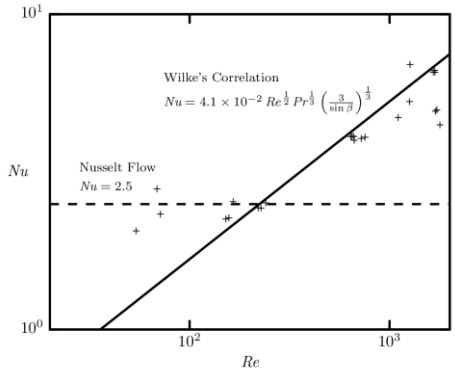

Figure 16: Mean flow Nusselt number Nu against the mean flow Reynolds number Re plot, compiled using data from different flow conditions spanning a range of pulsation amplitudes and frequencies for Pr = 5.4. Along with the experimentally derived data, the correlation produced by Wilke [21] is also plotted for the examined Re number range.

In Figure 17, the standard deviation of the HTC fluctuation σ_h normalized by the mean HTC h, is plotted against the standard deviation of the wave thickness σ_D normalized by the mean film thickness D for two pulsation frequencies; 1.8 Hz (106 rpm run) and 3.6 Hz (212 rpm run). Referring to either pulsation frequency data, it can be ascertained that higher HTC fluctuation intensities are associated with lower film thickness fluctuation intensities. This trend can be described for both pulsation frequency data sets by fitting power functions, suggesting that stronger waviness and mixing dampens down the oscillations in the HTC. By comparing the two data sets amongst each other, it can be observed that overall lower HTC fluctuation intensities ensue in the higher pulsation frequency run. Moreover, with increasing film thickness fluctuation intensities, the disparity in the HTC behaviour between the

higher wave frequency data and the lower wave frequency data diminishes.

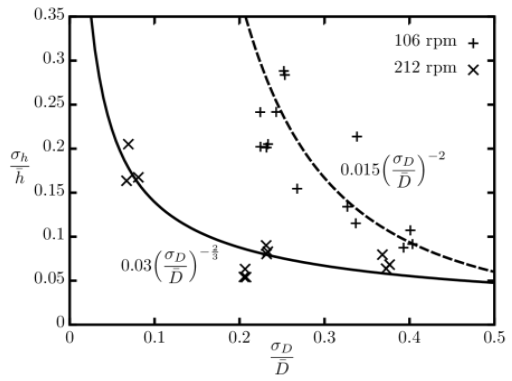

Figure 17: Fluctuation intensity of the HTC as a function of the normalised wave amplitude, with a 1.8 and 3.6 Hz (or, 106 and 212 rpm) pulsation in the flow.

Finally the effect of pulsation frequency on the interfacial wave velocity, the latter calculated from cross-correlations across successive film thickness profiles, was investigated for three different flow Re numbers in the 140 to 350 range. In these experiments, the forcing frequency was set to either 1.8 or 3.5 Hz. The results are presented in Figure 18.

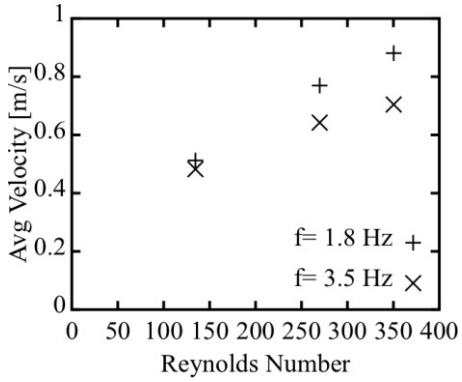

Figure 18: Average wave velocity plotted against mean flow Re numbers in the 140 – 350 range for two pulsation frequencies: 1.8 and 3.6 Hz.

As the flow Re varies from 140 to 350, the mean interfacial velocity increases in the 0.5 – 0.9 ms^{-1} range. Moreover, a near-liner trend can be identified despite the limited number of data points; a result that is expected given that the fluid viscosity and foil inclination angle remain unaltered, and consequently, the flow Re scales with the bulk flow velocity. Another interesting observation is that the relationship does not go through the origin. The underlying reason for this phenomenon is believed to be the superposition of the wave velocity with the bulk flow velocity. By comparing the two data sets amongst each other, it can finally be noted that the lower forcing frequency can be associated with higher interfacial velocities. This observation can be explained on the basis that higher excitation forcing frequencies produce shallower, smoother and slower waves compared to the larger and higher-dimensional waves associated with lower frequencies.

CONCLUSIONS

A combined PLIF/IR thermography technique was developed and employed in the experimental characterization of unsteady and conjugate heat transfer in gravity-driven liquid film flows down an inclined heated metal foil. The main challenge associated such measurements, and in particular the conjugation effects, is that the temperature variations at the film interfaces (solid-liquid and gas-liquid) must be measured directly and simultaneously in both space and time. Thus, simultaneous spatiotemporal measurements were pursued and are herein reported for the local and instantaneous film thickness, film free surface and substrate temperature, heat transfer coefficient, and heat flux exchanged between the heated foil and liquid film. Finally, interfacial wave velocities were calculated from cross-correlations across successive film thickness profiles and linked to the flow Re number at different pulsation frequencies and heat inputs. Following a qualitative assessment of the thermal features observed on the film free surface and foil underside throughout the experimental runs, a quantitative analysis was carried out with the ultimate goal of associating the observed flow dynamics with the heat transfer characteristics of these flows.

The heat transfer characteristics of film flows undergoing pulsation, such as the instantaneous and local heat transfer coefficient variation with the mean film thickness and film thickness fluctuation intensity, are of paramount significance as they can be used to assess the validity of the steady flow analysis. Despite describing the HTC enhancement at lower film thickness values reasonably well, while also capturing the overall trend, the novel results presented herein suggest that the magnitude of the true heat transfer coefficient is significantly higher, by up to a factor 2. A number of unsteady flow phenomena linked to the interface waviness of are believed to contribute towards this enhancement.

The average wave velocity was found to be in the range 0.5 – 0.9 m s^{-1}. The average Nu number increased with the mean flow Re number, while at low values (lowest flow-rates), a Nu of around 2.5 was observed, in agreement with laminar flow theory. Finally, lower wave amplitude intensities were associated with higher heat transfer coefficient fluctuation intensities (relative their respective means).

REFERENCES

[1] Mathie, R., Nakamura, H. and Markides, C. N., Heat transfer augmentation in unsteady conjugate thermal systems - Part II: Applications, International Journal of Heat and Mass Transfer, Vol. 56, 2013, pp. 819-833

[2] Mathie, R. and Markides, C. N., Heat transfer augmentation in unsteady conjugate thermal systems - Part I: Semi-analytical 1-D framework, International Journal of Heat and Mass Transfer, Vol. 56, 2013, pp. 802-818

[3] Brauner, N. and Maron, D. M., Characteristics of inclined thin films, waviness and the associated mass transfer, International Journal of Heat and Mass Transfer, Vol. 25, 1982, pp. 99-110
[4] Alekseenko, S., Nakoryakov, V. E. and Pakusaev, B. G., Wave effect on the transfer processes in liquid films, Chemical Engineering Communications, Vol. 141-142, 1996, pp. 359-385
[5] Mudawar, I. and Houpt, R. A., Measurement of mass and momentum transport in wavy-laminar falling liquid films, International Journal of Heat and Mass Transfer, Vol. 37, 1993, pp. 4151-4162
[6] Zadrazil, I., Matar, O. K. and Markides, C. N., An experimental characterization of downwards gas-liquid annular flow by laser-induced fluorescence: Flow regimes and film statistics, Int J Multiphase Flow, Vol. 60, 2014, pp. 87-102
[7] Dietze, G. F., Al-Sibai, F. and Kneer, R., Experimental Study of flow separation in laminar falling liquid flows, Journal of Fluid Mechanics, Vol. 637, 2009, pp. 73-104
[8] Schagen, A. and Modigell, M., Local film thickness and temperature distribution measurement in wavy liquid films with a laser-induced luminescence technique, Experiments in Fluids, Vol. 43, 2007, pp. 209-221
[9] Schagen, A., Modigell, M., Dietze, G. and Kneer, R., Simultaneous measurement of local film thickness and temperature distribution in wavy liquid films using a luminescence technique, International Journal of Heat and Mass Transfer, Vol. 49, 2006, pp. 5049-5061
[10] Nusselt, W., Die Oberflachenkondensation des Wasserdampfes, Z. Vereines Deutscher Ingenieure, Vol. 60, 1916, pp. 541-546
[11] Moran, K., Inumaru, J. and Kawaji, M., Instantaneous hydrodynamics of laminar wavy liquid films, Int J Multiphase Flow, Vol. 28, 2002, pp. 731-755
[12] Kabov, O. A., Scheid, B., Sharina, I. A. and Legros, J.-C., Heat transfer and rivulet structures formation in a falling thin liquid film locally heated, International Journal of Thermal Sciences, Vol. 41, 2002, pp. 664-672
[13] Chinnov, E. A. and Kabov, O. A., Marangoni Effect on Wave Structure in Liquid Films, Microgravity Science and Technology, Vol. 19, 2007, pp. 18-22
[14] Chinnov, E. A., Shatskii, E. N. and Kabov, O. A., Effect of Thermocapillary Pertrubations on the Wave Motion in in Heated Falling Liquid Film, Technical Physics Letters, Vol. 36, 2010, pp. 53-56
[15] Chinnov, E. A. and Shatskii, E. N., Evolution of the Temperature Field at the ThreeDimensional Wave Front in a Heated Liquid Film, Heat and Mass Transfer and Physical Gas Dynamics, Vol. 50, 2012, pp. 104-111
[16] Löffler, K., Yu, H., Hardt, S., Gambaryan-Roisman, T. and Stephan, P., Heat Transfer and Evaporation of Falling Liquid Films on Surfaces With Advanced Three-Dimensional Periodic Structures: Experiments and Numerical Simulations, ASME 2010 8th International Conference on Nanochannels, Microchannels, and Minichannels collocated with 3rd Joint US-European Fluids Engineering Summer Meeting, 2010, pp. 30761. 1-8
[17] Lel, V. V., Kellermann, A., Dietze, G., Kneer, R. and Pavlenko, A. N., Investigations of the Marangoni effect on the regular structures in heated wavy liquid films, Experiments in Fluids, Vol. 44, 2008, pp. 341-354
[18] Zhang, F., Wu, Y.-T., geng, J. and Zhang, Z.-B., An investigation of falling liquid films on a vertical heated/cooled plate, International Journal of Multiphase Flows, Vol. 34, 2008, pp. 13-28
[19] Zhang, F., Zhao, X., Geng, J., Wu, Y.-T. and Zhang, Z., A new insight into Marangoni effect in non-isothermal falling liquid films, Experimental Thermal and Fluid Science, Vol. 31, 2007, pp. 361-365
[20] Markides, C. N. and Mathie, R., Part I: Simultaneous PLIF-IR technique for Spatiotemporally resolved Heat Transfer Measurements in Unsteady and Conjugate Heated Falling Film Flows, 8th World Conference on Experimental Heat Transfer, Fluid Mechanics, and Thermodynamics Lisbon, Portugal, 2013, pp. 1-8
[21] Wilke, W., Warmeubergang an Rieselfilme, Forsch Hft. Ver. Dt. Ing, Vol. 490, 1962, pp.
[22] Yih, S. M., Modeling heat and mass transfer in wavy and turbulent falling liquid films, Wärme und Stoffübertragung, Vol. 21, 1987, pp. 373-381
[23] Miyara, A., Flow Dynamics and Heat Transfer of Wavy Condensate Film, Journal of Heat Transfer, Vol. 123, 2001, pp. 492-500